TiGePt – a study of Friedel differences

Ackerbauer, Sarah-Virginia ; Borrmann, Horst ; Bürgi, Hans-Beat ; Flack, Howard D ; Grin, Yuri ; Linden, Anthony ; Palatinus, Lukáš ; Schweizer, W Bernd ; Warshamanage, Rangana ; Wörle, Michael

Abstract: Abstract: The X-ray single-crystal diffraction intensities of the intermetallic compound TiGePt were analysed. These showed beyond doubt that the crystal structure is non-centrosymmetric. The analysis revolves around the resonant-scattering contribution to differences in intensity between Friedel opposites hkl and . The following techniques were used: Rmerge factors on the average (A) and difference (D) of Friedel opposites; statistical estimates of the resonant-scattering contribution to Friedel opposites; plots of 2Aobs against 2Amodel and of Dobs against Dmodel; the antisymmetric D-Patterson function. Moreover it was possible to show that a non-standard atomic model was unnecessary to describe TiGePt. Two data sets are compared. That measured with Ag K[alpha] radiation at 295 K to a resolution of 1.25 Å-1 is less conclusive than the one measured with Mo K[alpha] radiation at 100 K to the lower resolution of 0.93 Å-1. This result is probably due to the fact that the resonant scattering of Pt is larger for Mo K[alpha] than for AgK[alpha] radiation.

DOI: https://doi.org/10.1107/S2052519213021635

Acta Crystallographica Section B
Structural Science, Crystal Engineering and Materials
ISSN 2052-5192

TiGePt – a study of Friedel differences

Sarah-Virginia Ackerbauer, Horst Borrmann, Hans-Beat Bürgi, Howard D. Flack, Yuri Grin, Anthony Linden, Lukáš Palatinus, W. Bernd Schweizer, Rangana Warshamanage and Michael Wörle

Acta Cryst. (2013). B**69**, 457–464

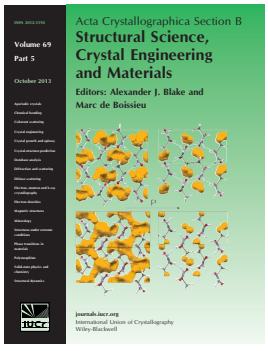

Acta Crystallographica Section B: Structural Science, Crystal Engineering and Materials publishes scientific articles related to the structural science of compounds and materials in the widest sense. Knowledge of the arrangements of atoms, including their temporal variations and dependencies on temperature and pressure, is often the key to understanding physical and chemical phenomena and is crucial for the design of new materials and supramolecular devices. *Acta Crystallographica B* is the forum for the publication of such contributions. Scientific developments based on experimental studies as well as those based on theoretical approaches, including crystal-structure prediction, structure–property relations and the use of databases of crystal structures, are published.

Acta Crystallographica Section B
Structural Science, Crystal Engineering and Materials
ISSN 2052-5192

TiGePt – a study of Friedel differences

Sarah-Virginia Ackerbauer,[a] Horst Borrmann,[a] Hans-Beat Bürgi,[b,c] Howard D. Flack,[d] Yuri Grin,[a]* Anthony Linden,[c] Lukáš Palatinus,[e] W. Bernd Schweizer,[f] Rangana Warshamanage[c] and Michael Wörle[g]

[a]Chemische Metallkunde, Max-Planck-Institut für Chemische Physik fester Stoffe, Nöthnitzer Strasse 40, D-01187 Dresden, Germany, [b]Departement für Chemie und Biochemie, Universität Bern, Freiestr. 3, CH-3012 Bern, Switzerland, [c]Institute of Organic Chemistry, University of Zürich, Winterthurerstrasse 190, CH-8057 Zürich, Switzerland, [d]Chimie minérale, analytique et appliquée, University of Geneva, Geneva, Switzerland, [e]Department of Structure Analysis, Institute of Physics, Czech Academy of Sciences, Cukrovarnicka 10, CZ-162 53 Prague, Czech Republic, [f]Laboratorium für Organische Chemie, ETH Zurich, Wolfgang-Pauli Strasse 10, CH-8093 Zürich, Switzerland, and [g]Laboratorium für Anorganische Chemie, ETH Zürich, HCI H103, Wolfgang-Pauli-Strasse 10, CH-8093 Zürich, Switzerland

Correspondence e-mail: grin@cpfs.mpg.de

Received 16 May 2013
Accepted 2 August 2013

The X-ray single-crystal diffraction intensities of the intermetallic compound TiGePt were analysed. These showed beyond doubt that the crystal structure is non-centrosymmetric. The analysis revolves around the resonant-scattering contribution to differences in intensity between Friedel opposites hkl and $\bar{h}\bar{k}\bar{l}$. The following techniques were used: $R_{\rm merge}$ factors on the average (A) and difference (D) of Friedel opposites; statistical estimates of the resonant-scattering contribution to Friedel opposites; plots of $2A_{\rm obs}$ against $2A_{\rm model}$ and of $D_{\rm obs}$ against $D_{\rm model}$; the antisymmetric D-Patterson function. Moreover it was possible to show that a non-standard atomic model was unnecessary to describe TiGePt. Two data sets are compared. That measured with Ag $K\alpha$ radiation at 295 K to a resolution of 1.25 Å^{-1} is less conclusive than the one measured with Mo $K\alpha$ radiation at 100 K to the lower resolution of 0.93 Å^{-1}. This result is probably due to the fact that the resonant scattering of Pt is larger for Mo $K\alpha$ than for Ag$K\alpha$ radiation.

1. Introduction

In their study of a structural transformation with negative-volume expansion of the intermetallic compound TiGePt, Ackerbauer *et al.* (2012) had considerable trouble deciding whether the space group of the low-temperature phase was centrosymmetric or not. Neutron powder diffraction was applied to the problem as the scattering lengths of Ti and Ge are markedly different. Supporting the experimental results with theoretical calculations, these authors were able to show conclusively that the crystal structure of the low-temperature (LT) phase of TiGePt is non-centrosymmetric. Ackerbauer *et al.* (2012) also studied the crystal structure of the high-temperature phase (> 1158 K) of TiGePt which surprisingly is 10% denser, and has a lower symmetry, than LT-TiGePt. Moreover, Ackerbauer *et al.* (2012) proposed a mechanistic model for the phase transformation between the low- and high-temperature phases.

In the current paper we have taken an alternative approach to the determination of the symmetry of LT-TiGePt. Single-crystal X-ray diffraction measurements are used and we deal principally with the analysis of the intensities of Friedel differences. The average and difference of Friedel opposites, both observed and model, are defined as follows: $A(hkl) = \frac{1}{2}[|F(hkl)|^2 + |F(\bar{h}\bar{k}\bar{l})|^2]$, $D(hkl) = |F(hkl)|^2 - |F(\bar{h}\bar{k}\bar{l})|^2$. Recent publications of particular relevance to the current paper are

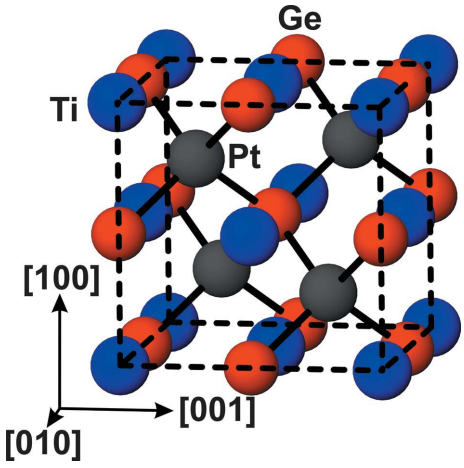

Figure 1
Crystal structure of LT-TiGePt. Ti, Pt and Ge atoms are shown as blue, grey and red spheres, respectively. The shortest Ge—Pt contacts have been drawn.

Flack *et al.* (2011), Parsons *et al.* (2012), Parsons *et al.* (2013) and other papers cited therein.[1]

LT-TiGePt crystallizes in the cubic MgAgAs-type structure. The latter can be regarded as a ternary ordered variant of the CaF_2 type. The Ti and Ge atoms are located at the positions of the F atoms, and the Pt atom on the Ca site, occupying one half of the tetrahedral voids. The Ti and Ge atoms have four Pt neighbours in a tetrahedral arrangement. The Pt atom is in a cubic environment, built up of two interpenetrating tetrahedra of Ti and Ge atoms. This structural arrangement is clearly displayed in Fig. 1. Ackerbauer *et al.* (2012) should be consulted for complete information on the crystal structures of TiGePt.

2. Data and structure

Two sets of intensity data were measured from the same crystal specimen and these are labelled Mo and Ag, respectively. The diffraction data set collected in Ackerbauer *et al.* (2012) was used here as the Ag data. Relevant characteristics are given in Table 1, which also includes the values of the resonant-scattering contributions for Ti, Ge and Pt. No evidence of twinning was found from the shape of the crystal. A semi-empirical absorption correction using spherical harmonics derived from an assessment of symmetry-equivalent intensities was applied to the intensity data. Fig. 2 shows the distributions of $|F|^2/u(|F|^2)$ against $\sin\theta/\lambda$, and illustrates the differences [absolute values of $|F|^2/u(|F|^2)$ and ranges of $\sin\theta/\lambda$] and similarities [decay of $|F|^2/u(|F|^2)$ and scatter at the same value of $\sin\theta/\lambda$] of the two data sets. $u(|F|^2)$ is the

Table 1
Experimental details for LT-TiGePt.

	Data set Mo	Data set Ag
Chemical formula	TiGePt	
M_r	315.58	
Crystal family, space group	Cubic, $F\bar{4}3m$	
Pearson symbol	*cF*12	
Z, formula units per cell	4	
Crystal shape, dimension (μm)	Prism, 20 × 20 × 30	
Crystal colour	Metallic black	
Crystal data		
a (Å)	5.9138 (3)	5.9349 (2)
V (Å^3)	206.824 (18)	209.05 (2)
f'(Ti), f'(Ge), f'(Pt)	0.2776, 0.1547, −1.7033	0.2060, 0.3016, −0.6812
f''(Ti), f''(Ge), f''(Pt)	0.4457, 1.8001, 8.3905	0.2830, 1.1903, 5.7081
Data collection		
Diffractometer	Bruker APEX-II	Rigaku R-AXIS Spider
Radiation	Mo *Kα*	Ag *Kα*
Temperature (K)	100	295
μ (mm^{-1})	995.2	477.9
T_{max}/T_{min}	1.42	1.23
R_{int} in $\bar{4}3m$	0.0354	0.0425
$\sin(\theta)/\lambda_{max}$ (Å^{-1})	0.93	1.25
Refinement		
$R[\|F\|^2 > 2u(\|F\|^2)]$	0.0087	0.031
No. of parameters	5	5
Reflection count		
	#Reflections [#sets]	#Reflections [#sets]
Measured	1761	864
Data merged and averaged in point group	$\bar{4}3m$	
Total	97	207
Paired acentric [pairs]	80 [40]	172 [86]
Centric (0*kl*, *hh*0, *h*00)	16	28
Unpaired acentric [pairs]	1 [1]	7 [7]
Data merged and averaged in point group	23	
Total	128	303
Complete sets of:		
4 $m\bar{3}m$ general *hkl*	44 [11]	148 [37]
2 $m\bar{3}m$ special 0*kl*	16 [8]	32 [16]
2 $m\bar{3}m$ special *hhl*	44 [22]	96 [48]
2 $m\bar{3}m$ special *hhh*	12 [6]	14 [7]
1 $m\bar{3}m$ special *hh*0	3 [3]	5 [5]
1 $m\bar{3}m$ special *h*00	5 [5]	7 [7]
Incomplete sets of:		
$m\bar{3}m$ general *hkl*	3 [1]	0 [0]
$m\bar{3}m$ special *hhl*	1 [1]	0 [0]
$m\bar{3}m$ special *hhh*	0 [0]	1 [1]

[1] This study arose in a singular way. The crystal of TiGePt used for structure determination by Ackerbauer *et al.* (2012) was submitted to the 2011 Zurich School of Crystallography (Linden & Buergi, 2008; http://www.chem.uzh.ch/linden/zsc) by one of the 20 student-participants (S.-V. Ackerbauer) as her project study. Diffraction measurements (Mo *Kα* radiation) were made by the school organizers and the student had to solve and refine the project structure, once two example structures provided by the school had been completed. The intermetallic compound TiGePt is atypical in its chemical composition and symmetry compared with most crystals submitted by the other student participants. At an *R* value of 1.1%, the study of TiGePt was still producing furrowed brows amongst the ten highly experienced tutors and the student. The values of statistics concerning the fit of Friedel opposites, described below, looked weird. In particular, it was not entirely clear whether the space group was non-centrosymmetric or not, and in the hustle and bustle of the school, there was no time to pursue these problems further. A lively e-mail discussion was undertaken following the school and its results are presented in this paper.

Table 2
Atomic coordinates and site occupancies in TiGePt, space group $F\bar{4}3m$.

Atom	Site	Site symmetry	Atom $x\ y\ z$	Fully ordered Ge	Site occupation Ti	Mixed-occupation Ge	Ti
Ti	4*a*	$\bar{4}3m$	0 0 0	0	1	$1-p$	p
Ge	4*b*	$\bar{4}3m$	$\frac{1}{2}\frac{1}{2}\frac{1}{2}$	1	0	p	$1-p$
Pt	4*c*	$\bar{4}3m$	$\frac{1}{4}\frac{1}{4}\frac{1}{4}$				

Table 3
TiGePt: $R_{\rm merge}$ values for the 11 (Mo) and 37 (Ag) sets of $m\bar{3}m$ general reflections which have all 4 equivalents hkl, $\bar{h}\bar{k}l$, khl, $\bar{k}\bar{h}\bar{l}$ in the data set.

$R_{\rm merge}$ (%)	$m\bar{3}m$	432	$\bar{4}3m$	$m\bar{3}$
$R_{\lvert F\rvert^2}$ (Mo)	1.53	1.35	1.05	1.41
$R_{\rm A}$ (Mo)	0.71	0.71	0.71	
$R_{\rm D}$ (Mo)	100	158	63.3	100
$R_{\lvert F\rvert^2}$ (Ag)	4.28	3.62	3.69	3.30
$R_{\rm A}$ (Ag)	2.74	2.74	2.74	
$R_{\rm D}$ (Ag)	100	102	98	100

standard uncertainty of $|F|^2$, see Schwarzenbach *et al.* (1995). The supplementary material[2] contains relevant data files: (i) hkl, $|F_{\rm obs}|^2$ and $u(|F_{\rm obs}|^2)$ merged and averaged in point group 23 for Mo $K\alpha$ at 100 K and Ag $K\alpha$ at 295 K, (ii) hkl, $|F_{\rm model}|^2$, $|F_{\rm obs}|^2$ and $u(|F_{\rm obs}|^2)$ merged and averaged in point group $\bar{4}3m$ for Mo $K\alpha$ at 100 K and Ag $K\alpha$ at 295 K.

The model of the ordered non-centrosymmetric crystal structure of TiGePt is described in the space group $F\bar{4}3m$ (No. 216), $Z = 4$, $a \simeq 5.92$ Å, with the atomic positions indicated in Table 2. All atomic coordinates are fixed on special positions and the atomic site symmetries force the harmonic atomic displacement parameters to be isotropic. Study of the phase diagram shows that the LT-TiGePt phase occurs at the equiatomic stoichiometric composition without any homogeneity range (Ackerbauer *et al.*, 2012). One must, however, allow for the partial mixed occupation of different crystallographic sites, in particular the possibility of some Ti atoms occupying the Ge site and some Ge atoms occupying the Ti site. For this case, one finds the appropriate site occupation parameters described in terms of the single parameter p shown in Table 2. A value of $p = 1$ corresponds to the fully ordered non-centrosymmetric structure. However, for $p = 1/2$ (with identical atomic displacement parameters on the Ge and Ti sites), the crystal structure has become effectively centrosymmetric, space group $Fm\bar{3}$m (No. 225), with Pt in site 4*b* and mixed Ge/Ti occupation of site 8*c* of that space group. To help in the further analysis of this structure, *Appendix A* gives the expressions for the average (A) and difference (D) Friedel intensities for the stoichiometric, fully occupied, non-centrosymmetric model structure. The Debye–Waller factors have not been included in these expressions. A least-squares refinement of the Mo data with variable p converges to a value of p close to unity, $p = 1.16$ (5), $U_{\rm Ti} = U_{\rm Ge} = 0.00206$ (6) Å^2 and $U_{\rm Pt} = 0.00169$ (3) Å^2.

[2] Supplementary data for this paper are available from the IUCr electronic archives (Reference: GP5067). Services for accessing these data are described at the back of the journal.

3. $R_{\rm merge}$ tests

Techniques exploiting the differences in intensities between Friedel opposites and based on the familiar $R_{\rm merge}$ ($R_{\rm int}$) values which attempt to detect the point group of the crystal are described in this section. These techniques are to be applied at the outset of a structure analysis when no atomic model of the crystal structure is available. Although full details are given in §3 of Parsons *et al.* (2012), it is useful to recall briefly the main results of that work. For the chiral (non-centrosymmetric) crystal structure of potassium hydrogen 2*R*,3*R* tartrate, it was found that whereas the $R_{\rm merge}$ values on $|F|^2$ weakly indicated the correct point group, the indications of those on D were unequivocally in favour of the chiral crystal structure. Moreover, the study of the centrosymmetric crystal structure of 1-methyl-4-oxotetrahydro-2*H*-imidazol-2-iminium tetrachloro-copper(II) showed almost identical $R_{\rm merge}$ values on either $|F|^2$ or D for all point groups in the Laue class. Most unfortunately, very few such studies have been undertaken and the literature does not provide helpful background information. Further, in studying Table 3 it should be noted that the $R_{\rm merge}$ value on D in a centrosymmetric point group is 100%, not by coincidence, but by definition.

The Laue class of TiGePt was assumed to be $m\bar{3}m$ so, according to Table 2 of Parsons *et al.* (2012), the data files of the observed intensities of TiGePt merged and averaged in point group 23 were obtained. The set of 4 reflections (hkl, $\bar{h}\bar{k}l$, khl, $\bar{k}\bar{h}\bar{l}$) are symmetry-equivalent in the point group $m\bar{3}m$

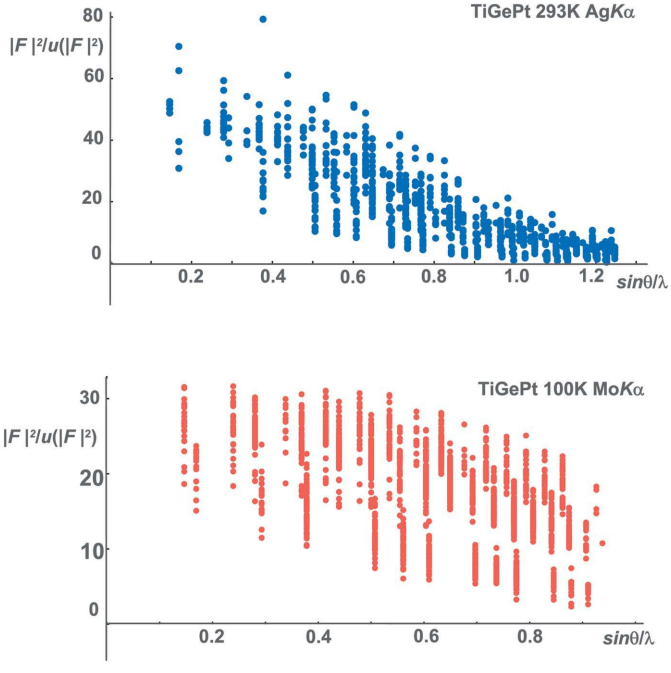

Figure 2
$|F|^2/u(|F|^2)$ plots for TiGePt illustrating the features of the data sets used for analysis. Top: Ag data set, bottom: Mo data set.

but not so in 23. The numbers of reflections and sets of reflections in the various classes of general and special reflections are given in detail in Table 1 (see the $m\bar{3}m$ entry in Table 1 of Parsons *et al.*, 2012, for the specification of the general and special reflections in $m\bar{3}m$). The number of incomplete sets of reflections is very small so the data sets were considered to be entirely satisfactory for the current analysis.

Table 3 shows the $R_{\rm merge}$ values for the 11 (Mo) and 37 (Ag) sets of $m\bar{3}m$ general reflections with all 4 measurements in the set. For TiGePt the $R_{\rm merge}$ values on the $|F|^2$ seem to indicate that the point group is $\bar{4}3m$ for the Mo data set and $m\bar{3}$ for the Ag data set. However, with the same data and calculating with D, it is very clear for the Mo data set that $\bar{4}3m$ is a better choice than $m\bar{3}$ or $m\bar{3}m$ as the point group of the crystal. The results of the Ag data set are inconclusive. No atomic model was used in coming to this conclusion but an inherent problem with TiGePt is the small number of data available.

4. Friedif

Flack & Bernardinelli (2008) have shown that the product u.Friedif$_{\rm stat}$ usually lies in the range of values between 6 and 10, where u is the standard uncertainty of the Flack parameter (Flack, 1983) and Friedif$_{\rm stat}$ is a statistical estimate of the ratio of the root-mean-square Friedel difference to the mean of the Friedel average. Friedif$_{\rm stat}$ is calculated using the chemical composition of the compound and the wavelength of the X-radiation and takes values for TiGePt of 733 with Mo $K\alpha$ radiation and 512 with Ag $K\alpha$ radiation. All Friedif values are given in Table 4. The best least-squares refinement with variable p and independent $U_{\rm Ge}$ and $U_{\rm Ti}$ produced a value of the Flack parameter, $x(u)$, of 0.08 (13) for the Mo data set and −0.04 (24) for the Ag data set. Consequently, for TiGePt we find u.Friedif$_{\rm stat}$ = 95 for Mo and = 123 for Ag, far outside the normal range of values of 6–10. One should seek to understand how this discrepancy might have occurred. It would seem that the values of Friedif$_{\rm stat}$ that have been used are too large. The theoretical derivation of Friedif$_{\rm stat}$ presumes a large number of general acentric Bragg reflections, atoms that are situated only in general positions without any pseudo-symmetry, and space group $P1$. None of these axioms applies to TiGePt. Flack & Shmueli (2007) derived the corresponding formulae for a structure in $P1$ with a centrosymmetric substructure. These show that with only one atom in a centrosymmetric arrangement in a host of non-centrosymmetrically arranged atoms, the value of Friedif$_{\rm stat}$ is unchanged, whereas for an entirely centrosymmetric structure, Friedif$_{\rm stat}$ becomes zero. The formulae for $A_{\rm model}$ and $D_{\rm model}$ (*Appendix A*) for the $\bar{4}3m$ model of TiGePt needed to calculate the Friedif$_{\rm model}$ show that acentric reflections with hkl all even have $D_{\rm model} = 0$ due to all atoms occupying special positions in the unit cell. Using these expressions, which take account of the atomic positions in the crystal structure, one calculates the Friedif$_{\rm model}$ values given in Table 4.

Section 2 of Parsons *et al.* (2012) presents a procedure to determine the status of centrosymmetry in a structure by the comparison of Friedif$_{\rm stat}$ with Friedif$_{\rm obs}$ derived from the measured diffraction intensities of acentric reflections. Friedif$_{\rm obs}$ for TiGePt was calculated using the procedure presented by Parsons *et al.* (2012). Values for both data sets are given in Table 4. The standard interpretation of a Friedif$_{\rm obs}$ much smaller than Friedif$_{\rm stat}$ is that the crystal structure is centrosymmetric or non-centrosymmetric but twinned by inversion in a proportion close to 50:50. An alternative interpretation, particularly appropriate to TiGePt, is that a large subset of the intensity data is derived from centrosymmetric projections of the crystal structure or from reflection classes whose Friedel differences happen to be zero as a consequence of special atomic positions. In addition, the average crystal structure of LT-TiGePt may lose its non-centrosymmetric character due to partially mixed occcupations of the Ti and Ge atomic sites.

Table 4
Friedif values for TiGePt from the Mo and Ag data sets.

	Mo data set	Ag data set
Friedif$_{\rm stat}$	733	512
Friedif$_{\rm model}$	80	51
Friedif$_{\rm obs}$ (all $m\bar{3}m$ general hkl)	18	67
Friedif$_{\rm obs}$ (hkl all even)	15	49
Friedif$_{\rm obs}$ (hkl all odd)	19	83

In all, these approaches show that the diffraction data of TiGePt have a strong centrosymmetric contribution, and leaves the nagging doubt that the crystal structure of TiGePt might indeed be centrosymmetric.

5. AD and $D_{\rm obs}$ against $D_{\rm model}$ plots

Flack *et al.* (2011) introduced the $D_{\rm obs}$ against $D_{\rm model}$ plot as a means of validating the intensity data and structural model of a non-centrosymmetric crystal structure. Parsons *et al.* (2012) have improved this technique in the $2AD$ plot. Satisfactory plots of $D_{\rm obs}$ against $D_{\rm model}$ and $2A_{\rm obs}$ against $2A_{\rm model}$ show data points distributed about a straight line of slope 1 passing through the origin. Data sets for which the $D_{\rm obs}$ values are dominated by random uncertainties and systematic error show a $D_{\rm obs}$ against $D_{\rm model}$ plot where the data points are arranged along the $D_{\rm obs}$ axis at $D_{\rm model} = 0$. The latter distribution is also shown by centrosymmetric structures. To assess the overall fit of the data, the figures also include $D_{\rm obs} - D_{\rm model}$ and $2A_{\rm obs} - 2A_{\rm model}$ values of all reflections, displayed at constant abscissa. These hence show the spread of the deviations of $2A$ and D, and represent the uncertainties on the individual measurements achieved by the structure refinement.

For TiGePt, the plots of $A_{\rm obs}$ against $A_{\rm model}$ for the two data sets display the required distribution of points about a straight line of slope 1 passing through the origin. The domain of values of $|D_{\rm obs}|$ does not overlap that of $2A_{\rm obs}$ as is usually the case. To make the presentation of the $2AD$ plot as meaningful and as clear as possible, we chose to plot only the $2A_{\rm obs}$, $2A_{\rm model}$ data points of the 9 reflections with the lowest value of $2A_{\rm obs}$. All of these 9 weak reflections had hkl all even with $h + k + l = 4n + 2$. In this way the overall form both of $D_{\rm obs}$,$D_{\rm model}$ and of the weak $2A_{\rm obs}$,$2A_{\rm model}$ data points can be

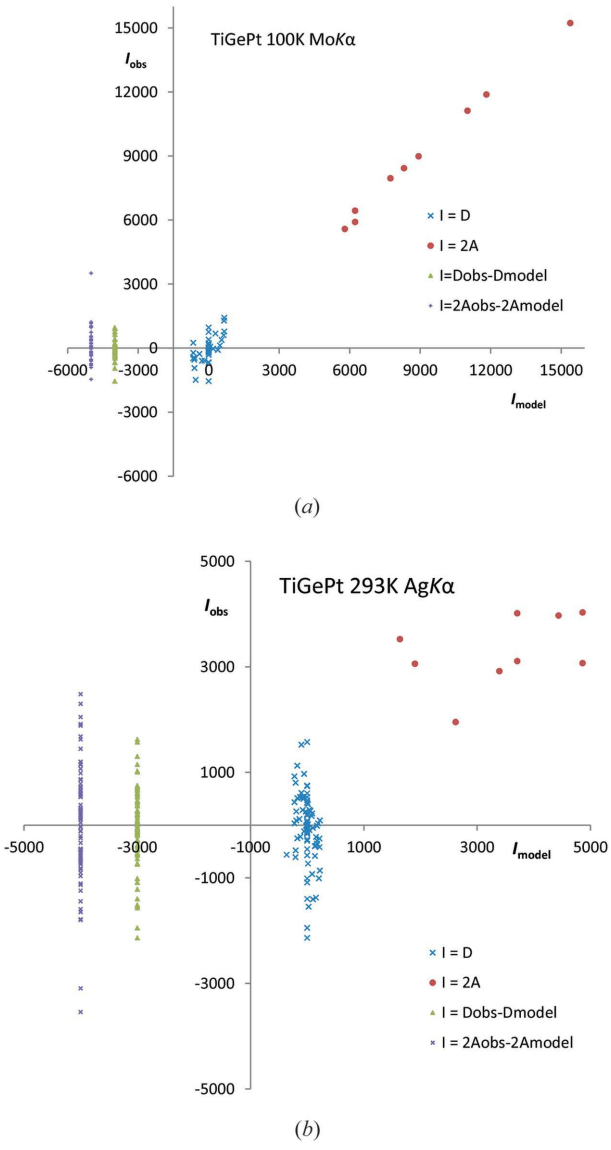

Figure 3
$2AD$ plots of TiGePt showing $2A_{obs}$ against $2A_{model}$ for the 9 weakest reflections and D_{obs} against D_{model} for all Friedel pairs. On the left of the plot, $D_{obs} - D_{model}$ and $2A_{obs} - 2A_{model}$ values of all reflections are displayed at constant abscissa. (*a*) Mo data set; (*b*) Ag data set. See footnote to §5.

seen. The plots are drawn for the structure refinement with fixed $p = 1$ and independent variables U_{Ge} and U_{Ti}. The $2AD$ plots are shown in Fig. 3. For the Mo data set, the fit of $2A_{obs}$ to $2A_{model}$ is good even for the 9 weak reflections, whereas that of the Ag data set is much less satisfactory.[3]

Fig. 4 shows the D_{obs} against D_{model} parts of Fig. 3 magnified. The acentric reflections fall into two distinct classes according to their reflection indices as expected from the formulae for D_{model} given in *Appendix A*. In the first class, *hkl* all even, the data points for the Mo data set in Fig. 4(*a*), are distributed along the line $D_{model} = 0$ as though they were centric reflections. In the second class, *hkl* all odd, with some imagination, one could say that the data points follow the ideal line of slope 1 passing through the origin. The basis for this interpretation is that a very large proportion of the data points lie in the first and third quadrants. The spread of the *hkl* all odd reflections is very wide. The domain of $|D_{obs}|$ values in the two classes is approximately the same suggesting that the same random uncertainties and systematic errors affect both classes. In the *hkl* all odd class, the domain of $|D_{obs}|$ values is approximately twice that of $|D_{model}|$ indicating the presence of systematic errors in these intensity data. For the Ag data set in Fig. 4(*b*), one sees no fit between D_{obs} and D_{model}, the range of $|D_{model}|$ values being much smaller than that of $|D_{obs}|$. *R* values are given in Table 5. For comparison the lowest R_D value that we have found to date in other studies is 29% (Flack, 2013). The D_{obs} against D_{model} plot from a refinement with $p = 1/2$

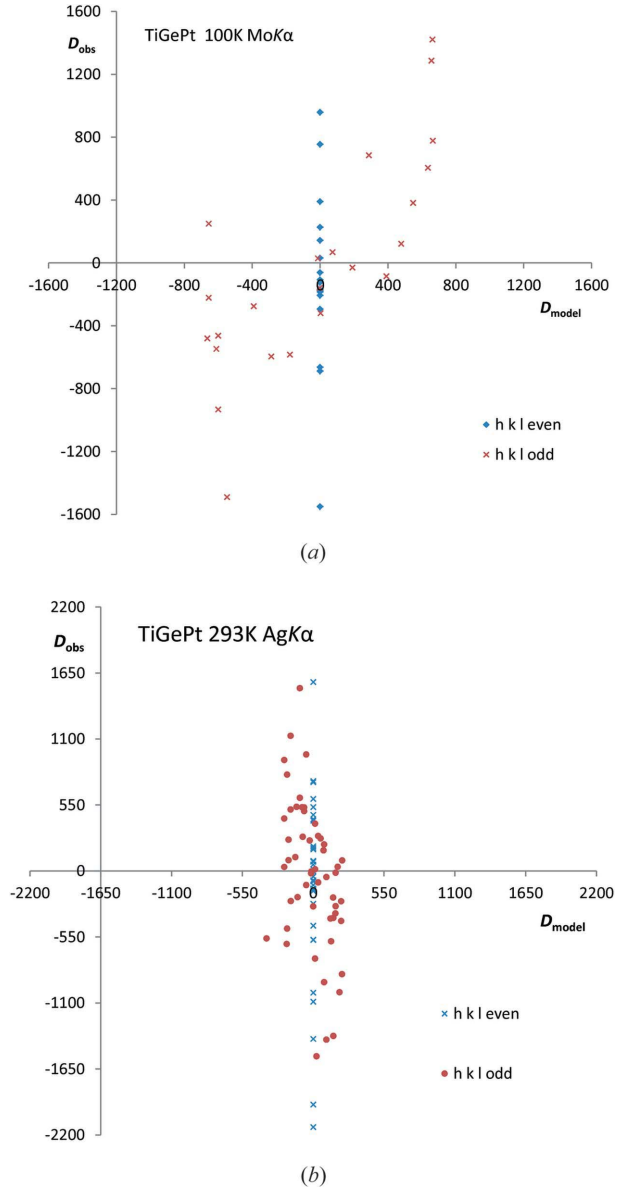

Figure 4
D_{obs} against D_{model} of TiGePt. (*a*) Mo data set; (*b*) Ag data set. See footnote to §5.

[3] It is arbitrary whether the $D_{obs}(hkl),D_{model}(hkl)$ data point is plotted as $D_{obs}(hkl),D_{model}(hkl)$ or as $D_{obs}(\underline{hkl}),D_{model}(\underline{hkl}) = -D_{obs}(hkl), -D_{model}(hkl)$. Indeed both points could be plotted. In Figs. 3 and 4, just one point corresponding to *hkl* with all positive integers has been plotted.

Table 5
R values for the Mo and Ag data sets of TiGePt.

R values in %	Mo data set	Ag data set
R_A	1.13	4.53
R_{Aweak}	1.72	27.7
R_D all acentric pairs	76.8	109
R_D acentric pairs with *hkl* all even	100	100
R_D acentric pairs with *hkl* all odd	63.6	115

Table 6
Interatomic vectors in the structure of TiGePt.

Vector	Atom pairs
[0 0 0]	Ti → Ti, Ge → Ge, Pt → Pt
$[\frac{1}{4}\ \frac{1}{4}\ \frac{1}{4}]$	Ge → Pt, Pt → Ti
$[-\frac{1}{4}\ -\frac{1}{4}\ -\frac{1}{4}]$	Pt → Ge, Ti → Pt
$[\frac{1}{2}\ \frac{1}{2}\ \frac{1}{2}]$	Ti → Ge, Ge → Ti

and independent variables $U(0,0,0)$ and $U(\frac{1}{2},\frac{1}{2},\frac{1}{2})$ looks similar to Fig. 4(*a*) with like *R* values, whereas with $p = \frac{1}{2}$ and $U(0,0,0) = U(\frac{1}{2},\frac{1}{2},\frac{1}{2})$, all reflections have $D_{model} = 0$ and the structure is centrosymmetric.

In a similar way to the results of §4, the D_{obs} against D_{model} plots do not contain convincing evidence that the structure is really non-centrosymmetric. Changes in the value of *p*, U_{Ge} and U_{Ti} can drastically modify the appearance of the plot to the point of making it like that of a centrosymmetric crystal.

6. Necessity of a non-standard model

In the intensity data of TiGePt, there are sets of reflections of identical value of $h^2 + k^2 + l^2$, *e.g.* for $h^2 + k^2 + l^2 = 99$ there are the following three reflections: 339, 177 and 557. In the expressions for *A* and *D* of the standard model given in *Appendix A*, the reflections in these sets have identical values of A_{model} and $|D_{model}|$. Any departure in the corresponding observed values from this equality indicates that the real crystal structure deviates from the standard model by way of either complex static atomic displacements, or anharmonic thermal motion or non-spherical atomic electron density. Despite the small number of such sets of reflections we have nevertheless analysed the corresponding observed values. The R_{merge} evaluates to 0.83% (Mo) and 3.13% (Ag). These values are slightly less than the R_{int} of each whole data set and indicate that there is no need to extend the model beyond the standard one.

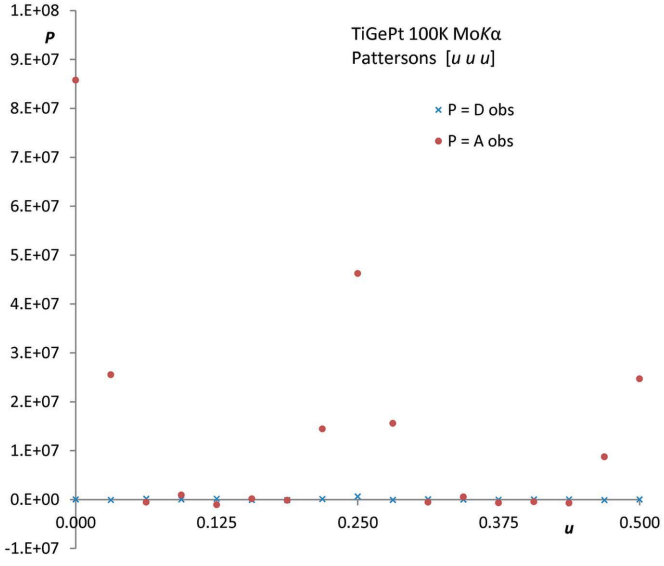

Figure 5
A_{obs}- and D_{obs}-Patterson maps of TiGePt along the line [*u u u*]. Mo data set.

7. *A*- and *D*-Patterson functions

Background information on the *A*- and *D*-Patterson functions is given in §6 of Flack *et al.* (2011). Suffice it to say that both show the positions of interatomic vectors in the crystal structure. The *A*-Patterson function is centrosymmetric, it is calculated with the average intensity of Friedel opposites (*hkl* and $\bar{h}\bar{k}\bar{l}$) and it has peaks with a height determined essentially by Z_iZ_j, where Z_i is the atomic number of atom *i*. Consequently one sees all interatomic vectors in an *A*-Patterson map. The *D*-Patterson function is antisymmetric, it is calculated with the difference intensity of Friedel opposites and it has peaks with a height determined by $(f_if_j'' - f_jf_i'')$ where f_i and f_i'' are the real and imaginary components of the atomic scattering factor of atom *i*. Consequently, one only sees interatomic vectors between atoms of different chemical elements in a *D*-Patterson map. The value of a *D*-Patterson function of a centrosymmetric structure is zero everywhere.

The coordinates of the atoms in the structure of TiGePt given in Table 2 imply the interatomic vectors given in Table 6. All of them appear along [*u u u*] and consequently the *A*- and *D*-Patterson functions have been calculated only along this line.

Fig. 5 shows the A_{obs}- and D_{obs}-Patterson functions of TiGePt along the line [*u u u*] for the Mo data set. The A_{obs}-Patterson map shows large peaks at $u = 0.0$, corresponding to the Ge → Ge, Ti → Ti and Pt → Pt self-vectors; at $u = 0.25$, corresponding to the Pt → Ge and Pt → Ti vectors; and at $u = 0.5$, corresponding to the Ti → Ge vectors, see Table 6. In the intermediate regions, the A_{obs}-Patterson map is close to the background level of zero. One notes that the D_{obs}-Patterson map is also close to zero on the scale of the A_{obs}-Patterson function and one cannot discern its structure in Fig. 5. A plot (not shown) of the A_{model}- and D_{model}-Patterson maps for a non-centrosymmetric fully ordered model of TiGePt is essentially identical to Fig. 5, confirming the main details of the structural model.

Fig. 6 shows the D_{obs}- and D_{model}-Patterson map of TiGePt along the line [*u u u*] for the Mo data set. The model is that of the non-centrosymmetric and fully ordered structure. There is just one peak in the D_{obs}-plot at $u = 0.25$, corresponding to the Ge → Pt and Pt → Ti interatomic vectors. There is no peak at [0 0 0] as the interatomic vectors at this point are self-vectors of zero height in a *D*-Patterson function. Likewise there is no

peak at $[\frac{1}{2}\,\frac{1}{2}\,\frac{1}{2}]$ as this point contains contributions from the Ti → Ge and Ge → Ti vectors which annihilate one another. The rest of the D_{obs}-Patterson map is a noisy background rising to its largest value of $|P|$ of 137 066, about 20% of the peak value 620 750 at $u = 0.25$. The D_{model}-Patterson map has a peak at the same place as the D_{obs}-Patterson map (at $u = 0.25$) and with the same height within experimental uncertainty. There is thus excellent agreement between the observed and model Patterson functions for the Mo data set. Unsurprisingly, the background of the D_{model}-Patterson map is less noisy than that of the D_{obs}-Patterson. The observation of the peak at $u = 0.25$ in the D_{obs}-Patterson map is most significant. This peak would occur neither with a centrosymmetric structure nor with a non-centrosymmetric crystal twinned by inversion in a ratio close to 50:50. The D_{obs}-Patterson map proves beyond doubt that the crystal structure is non-centrosymmetric, space group $F\bar{4}3m$, and the crystal measured is not twinned by inversion. The non-centrosymmetric fully ordered model reproduces this peak entirely satisfactorily.

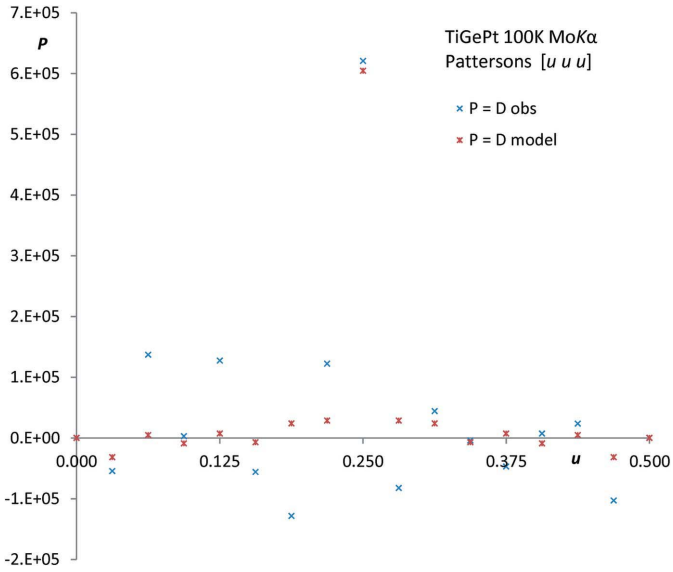

Figure 6
D_{obs}- and D_{model}-Patterson maps of TiGePt along the line $[u\,u\,u]$. Mo data set.

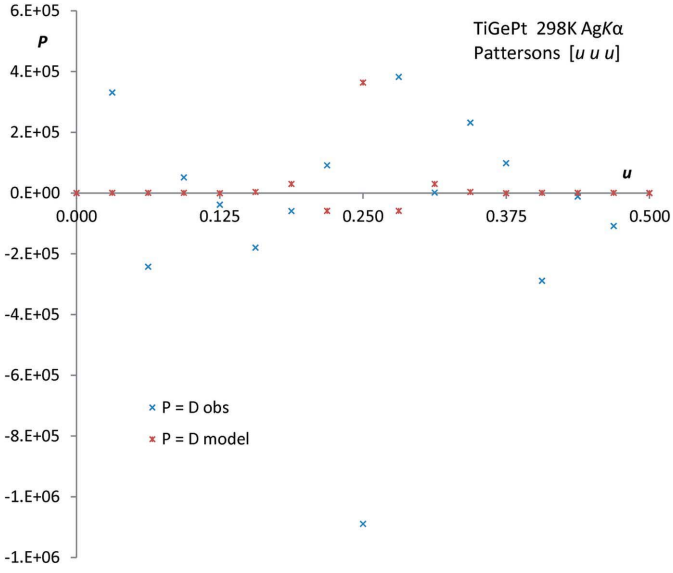

Figure 7
D_{obs}- and D_{model}-Patterson maps of TiGePt along the line $[u\,u\,u]$. Ag data set.

For the Patterson maps calculated from the Ag data set, the D_{obs} and A_{obs} plots (not shown) correspond very closely to those presented in Fig. 5. Likewise the D_{model} and A_{model} plots (not shown) correspond very closely to those from the Mo data set. However, the D_{obs}-Patterson map for the Ag data set shown in Fig. 7 is far more noisy than that in Fig. 6 for the Mo data. This is often observed in residual density maps and is most probably caused by the larger range of $\sin\theta/\lambda$. Also reference to Table 1 shows a large difference in f'' of Pt for the two radiations. One could not conclude from Fig. 7 that the structure is definitely non-centrosymmetric.

8. Concluding remarks

For the intermetallic compound TiGePt with a non-centrosymmetric space group but atoms in positions of high point symmetry, statistics that are based only on observed values of D give the most reliable results in indicating whether the crystal structure is non-centrosymmetric or not. In particular, we note that the R_{merge} on A_{obs} and D_{obs} of complete sets of $m\bar{3}m$ general reflections and the D-Patterson maps work very well with the Mo data. These unequivocally indicate that the structure is non-centrosymmetric.

The ordered picture of the structure of TiGePt (*i.e.* the non-centrosymmetric one) is further supported by coherent-potential approximation (CPA) calculations of the band structure, which reveal a significantly higher energy of 1.2 eV per formula unit for the disordered structure in the space group $Fm\bar{3}m$ (Ackerbauer *et al.*, 2012).

The results presented in the current paper confirm the contention of Flack *et al.* (2011) that the A- and D-Patterson maps are useful techniques to employ in the validation of a crystal-structure determination. In general, peaks and troughs occurring at identical positions in an $A_{obs} - A_{model}$ and a $D_{obs} - D_{model}$ Patterson map of a crystal-structure determination are strong indications of some weakness in the structural model. The major current handicap to the use of these Patterson functions is the lack of software.

From the evidence presented in this paper, one discerns a distinct difference in the potentialities of the data set measured at 100 K with Mo $K\alpha$ radiation from that at 295 K with Ag $K\alpha$ radiation. Ag $K\alpha$ is a natural choice for a heavy element compound with a small unit cell if the atomic parameters, both positional and displacement, are of prime interest. However, this data, due to the lower resonant scattering especially for Pt (see Table 1), does not lead to a viable study of the absolute structure. With Mo $K\alpha$ radiation one can make good use of the intensity differences between Friedel

opposites, even though there are fewer data for determining the atomic parameters. Thus, with the data available to this study, one sees that some techniques make a clearer distinction than others between two models. Moreover, the present work also suggests that for a problem as difficult as deciding whether TiGePt is centrosymmetric or not, a more conclusive answer requires up to three experiments at the absorption edges of Pt, Ti and Ge rather than higher resolution data at a single wavelength. Such additional experiments are beyond the scope of the current paper.

APPENDIX *A*
Expressions for $A_{\rm model}$ and $D_{\rm model}$ for stoichiometric TiGePt with fully occupied sites

$$H = h + k + l \tag{1}$$

$$f = f^{\rm o} + f' \tag{2}$$

$$\phi_{\rm GT} = (2p - 1)\left(f_{\rm Ge} - f_{\rm Ti}\right) \tag{3}$$

$$\phi''_{\rm GT} = (2p - 1)\left(f''_{\rm Ge} - f''_{\rm Ti}\right) \tag{4}$$

$$A(H = 4n) = \left[f_{\rm Pt} + f_{\rm Ge} + f_{\rm Ti}\right]^2 + \left[f''_{\rm Pt} + f''_{\rm Ge} + f''_{\rm Ti}\right]^2 \tag{5}$$

$$D(H = 4n) = 0 \tag{6}$$

$$A(H = 4n + 2) = \left[f_{\rm Pt} - f_{\rm Ge} - f_{\rm Ti}\right]^2 + \left[f''_{\rm Pt} - f''_{\rm Ge} - f''_{\rm Ti}\right]^2 \tag{7}$$

$$D(H = 4n + 2) = 0 \tag{8}$$

$$A(H = 4n + 1) = f^2_{\rm Pt} + \phi^2_{\rm GT} + f''^2_{\rm Pt} + \phi''^2_{\rm GT} \tag{9}$$

$$D(H = 4n + 1) = 4f_{\rm Pt}\phi''_{\rm GT} - 4\phi_{\rm GT}f''_{\rm Pt} \tag{10}$$

$$A(H = 4n - 1) = f^2_{\rm Pt} + \phi^2_{\rm GT} + f''^2_{\rm Pt} + \phi''^2_{\rm GT} \tag{11}$$

$$D(H = 4n - 1) = -4f_{\rm Pt}\phi''_{\rm GT} + 4\phi_{\rm GT}f''_{\rm Pt} \tag{12}$$

References

Ackerbauer, S. V. *et al.* (2012). *Chem. Eur. J.* **18**, 6272–6283.
Flack, H. D. (1983). *Acta Cryst.* A**39**, 876–881.
Flack, H. D. (2013). *Acta Cryst.* C**69**, 803–807.
Flack, H. D. & Bernardinelli, G. (2008). *Acta Cryst.* A**64**, 484–493.
Flack, H. D., Sadki, M., Thompson, A. L. & Watkin, D. J. (2011). *Acta Cryst.* A**67**, 21–34.
Flack, H. D. & Shmueli, U. (2007). *Acta Cryst.* A**63**, 257–265.
Linden, A. & Buergi, H.-B. (2008). *Acta Cryst.* A**64**, C30.
Parsons, S., Flack, H. D. & Wagner, T. (2013). *Acta Cryst.* B**69**, 249–259.
Parsons, S., Pattison, P. & Flack, H. D. (2012). *Acta Cryst.* A**68**, 736–749.
Schwarzenbach, D., Abrahams, S. C., Flack, H. D., Prince, E. & Wilson, A. J. C. (1995). *Acta Cryst.* A**51**, 565–569.